


Article

Orange Peel Biochar–CdS Composites for Photocatalytic Hydrogen Production

Xiang Li ^{1,2,3}, Yuxin Zang ², Jindi Zhang ¹, Lili Zhang ¹, Jing Zhang ², Mengyang Huang ^{1,*} and Jiaqiang Wang ^{1,2,3,*} 

¹ School of Chemistry and Resources Engineering, Honghe University, Mengzi 661100, China; lx1535655417@163.com (X.L.); zhangjindi@uoh.edu.cn (J.Z.); zhanglili@uoh.edu.cn (L.Z.)

² School of Materials and Energy, Chemical Sciences & Technology, Institute of International Rivers and Eco-Security, Yunnan University, Kunming 650091, China; 458451215@163.com (Y.Z.); quayjing@163.com (J.Z.)

³ Institute of Frontier Technologies in Water Treatment Co., Ltd., Kunming 650503, China

* Correspondence: huangmengyang@uoh.edu.cn (M.H.); jqwang@ynu.edu.cn (J.W.)

Abstract: Orange peel biochar (C)-supported cadmium sulfide composites (CdS-C) were prepared by the combination of hydrothermal and calcination methods. The structure and morphology were characterized in detail by X-ray diffraction (XRD) and scanning electron microscopy (SEM), respectively. The CdS-C composite with 60% CdS exhibited the highest photocatalytic hydrogen production rate of 7.8 mmol·g⁻¹·h⁻¹, approximately 3.69 times higher than that of synthesized CdS without biochar. These results indicate that biochar derived from orange peel could be a low-cost, renewable, environmentally friendly, and metal-free co-catalyst for CdS, enhancing its photostability.

Keywords: photocatalytic hydrogen production; biochar; CdS; hydrothermal method



Citation: Li, X.; Zang, Y.; Zhang, J.; Zhang, L.; Zhang, J.; Huang, M.; Wang, J. Orange Peel Biochar–CdS Composites for Photocatalytic Hydrogen Production. *Inorganics* **2024**, *12*, 156. <https://doi.org/10.3390/inorganics12060156>

Academic Editor: Hicham Idriss

Received: 31 March 2024

Revised: 26 May 2024

Accepted: 28 May 2024

Published: 31 May 2024



Copyright: © 2024 by the authors. Licensee MDPI, Basel, Switzerland. This article is an open access article distributed under the terms and conditions of the Creative Commons Attribution (CC BY) license (<https://creativecommons.org/licenses/by/4.0/>).

1. Introduction

Among the existing renewable energy options, hydrogen is a clean, efficient, safe, and sustainable secondary energy source. It is currently recognized as the most ideal energy carrier and is considered the most promising new energy source of the 21st century. Solar energy, if effectively collected, converted, and stored, can be the greenest and most abundant energy source on Earth [1]. Among existing technologies, the use of visible light to activate photocatalytic reactions in semiconductor materials is considered one of the most promising and revolutionary approaches for addressing environmental pollution and meeting the challenges posed by global energy shortages [2].

The development of non-precious metal photocatalytic materials has long been an urgent need for fuel production and environmental treatment. Non-metallic carbon materials have proven to be a promising alternative as co-catalysts due to their low cost, ecological compatibility, good electrical conductivity, chemical stability, and photothermal effects [3–5]. Biomass-derived charcoal is an environmentally friendly material that is efficient, cheap, and easy to prepare. It has received widespread attention in the fields of materials science, chemistry, and environmental protection [6–9]. Biochar has a high specific surface area, high porosity, and sufficient surface functional groups. Its excellent ion exchange capacity and high stability make it a suitable material for pollution control [10]. To date, biochar materials from agricultural waste have been introduced for the preparation of composites for the photocatalytic removal of organic pollutants from water as well as for the production of hydrogen through water decomposition, supercapacitors, fuel cells, CO₂ adsorption, and energy storage [11–14]. More importantly, the synergistic effect of biochar with other metals or metal oxides can enhance the adsorption capacity of biochar-based catalysts, increase the visible light absorption, improve the separation of photogenerated electrons and holes, and reduce the bandgap, thereby improving the photocatalytic performance of biochar-based catalysts [15–18]. For example, biochar serves as the charge transfer mediator between Ag₃PO₄ and Fe₃O₄ and hinders the recombination

of electron–hole pairs (e^- - h^+). The efficient separation of e^- - h^+ pairs minimizes recombination, thereby boosting charge transfer and separation, which significantly improves the photocatalytic ability of biochar-based catalysts [19]. Modified biochar has been used as a substrate to anchor g - C_3N_4 - $FeVO_4$ heterojunctions to extend charge lifetime and enhance the adsorption capacity of the composites. Using a g - C_3N_4 - $FeVO_4$ -BC ternary system effectively achieved 98.4% removal of methylparaben degradation via adsorption-assisted photocatalysis [20].

Cadmium sulfide (CdS) is an inorganic compound with a narrow bandgap semiconductor material that absorbs most of the visible light in the spectrum. Its appropriate band edge position provides a good visible light absorption ability and excellent photoelectric conversion characteristics, making it widely used in ion detection, sensors, photocatalysis, and other fields [21–29]. In terms of optical properties, CdS still has room for exploration. For example, Yoichi Kobayashi et al. [30] used femtosecond transient absorption spectroscopy to investigate the effects of surface defect states and surface capping reagents on Auger recombination in CdS quantum dots (QDs). They claim that Auger recombination in CdS QDs does not depend on interfacial electronic structures originating from the surface defects and capping reagents of one monolayer level. In addition, Saptarshi Chakraborty et al. [31] used extended X-ray absorption fine structure spectroscopy to study dopant-induced structural perturbations and femtosecond transient absorption (TA) spectroscopy to study ultrafast charge-carrier dynamics, demonstrating that the ionic radius and the dopant oxidation state play a crucial role in determining the dopant anion bond lengths.

CdS also has disadvantages to a certain extent. Its photogenerated carriers are prone to recombination and susceptible to photocorrosion, significantly restricting their widespread application [32]. On the other hand, constructing heterojunctions can effectively promote charge separation, improve photocatalytic performance, and enhance the stability of photocatalytic materials [33]. Therefore, how to modify CdS by incorporating other non-precious metals or biomass charcoal is a compelling research direction. For example, by controlling the oxidation and reduction sites of the CdS/CdSe heterostructure, Rajesh Bera et al. [34] achieved a maximum H_2 generation of $5125 \mu\text{mol/g/h}$ for a 27.5 wt% CdSe-loaded CdS heterostructure, which was found to be 44 times higher than that of bare CdS nanorods and 22 times higher than that of CdSe nanoparticles.

Moreover, it is important to improve the photostability of CdS. A number of methods have been used to solve this problem, including metal ion doping [35–37], compounding with other semiconductors [38,39], and introducing co-catalysts [40,41]. In recent years, scientists have introduced the use of carbon-based materials such as biochar. Due to their high specific surface area and sufficient surface functional groups, they are considered one of the most effective methods to improve the performance of CdS in photocatalytic hydrogen production [42,43]. For example, the nanocomposites of mesoporous carbon and CdS nanoparticles have been shown to improve photostability and minimize photocorrosion of CdS. The introduction of mesoporous carbon prevents the recombination of photogenerated electrons and holes, thus avoiding photocorrosion in CdS and improving the stability and photocurrent response of the material [44]. Shi et al. [45] prepared a novel biochar-loaded CdS/ TiO_2 photocatalyst (CdS/ TiO_2 /BC) for glucose photoreforming using a simple hydrothermal and calcination method. The as-synthesized CdS/ TiO_2 /BC exhibited excellent acetic acid selectivity (63.94%) together with improved H_2 generation ($\sim 12.77 \text{ mmol}\cdot\text{g}^{-1}\cdot\text{h}^{-1}$) in 25 mM NaOH solution, while efficient formic acid selectivity (60.29%) and H_2 generation ($\sim 10.29 \text{ mmol}\cdot\text{g}^{-1}\cdot\text{h}^{-1}$) were observed in 3 mM Na_2CO_3 solution.

In this work, a biochar-supported cadmium sulfide (CdS-C) composite photocatalyst is prepared by a hydrothermal method combined with calcination using biochar as a support. A series of characterization analyses are carried out on the prepared samples and the visible light hydrogen production activity is evaluated. The optical and photoelectric properties of as-prepared photocatalysts are also characterized here. The aim of this work is to provide a facile pathway for constructing CdS photocatalytic systems for photocatalytic water decomposition for hydrogen production.

2. Results and Discussion

2.1. Synthesis and Characterizations

CdS–biochar-based composites are usually synthesized by a combined hydrothermal and calcination method [46–52]. In contrast, in this work, orange peel biochar-supported cadmium sulfide composites (CdS-C) were prepared by a combined hydrothermal and calcination method without adding any activation agent.

The XRD patterns of pure CdS and the CdS-xC ($x = 20, 40, 60, 80$) series of composites are shown in Figure 1, where x represents the amount of biomass char. It can be seen that the peak positions are similar across all samples. Peaks at 26.44° , 43.74° , and 51.82° correspond to the 75-1546 cubic phase, while peaks at 24.87° and 28.09° correspond to the 77-2306 hexagonal phase of the mixed crystalline form [53–55]. After incorporating orange peel biochar into pure CdS, the peak positions remained largely unchanged, though the intensity varied slightly. This indicates that while the crystal structure of the CdS remained unaltered, the crystallinity was affected to varying degrees by the addition of biochar.

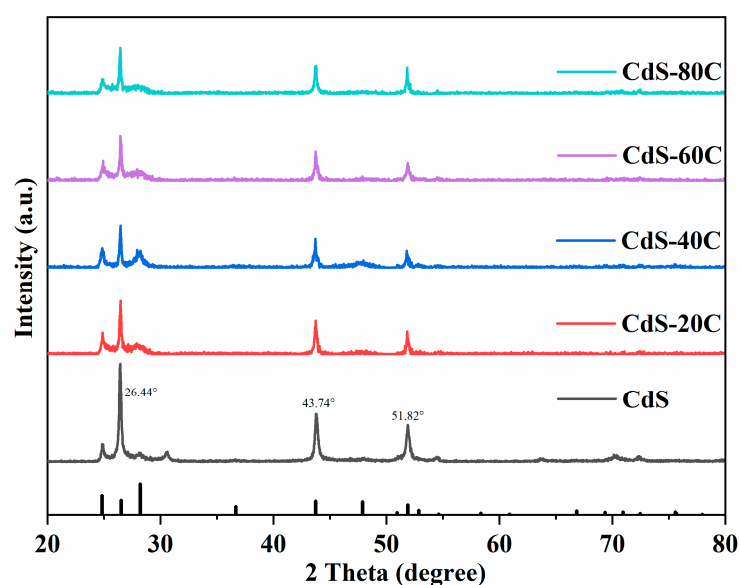


Figure 1. XRD patterns of CdS and CdS-xC ($x = 20, 40, 60, 80$).

The specific surface area of photocatalytic materials is crucial as it influences their physical adsorption properties [56]. Figure 2a shows the adsorption–desorption isotherm of N_2 on the CdS material, and Figure 2b shows the adsorption–desorption isotherm of N_2 on the CdS-60C material. The addition of orange peel biochar caused slight modifications on the surface of the CdS-C composite materials. This may be attributed to the alkaline etching treatment, which increased the pore density of the biochar, thereby enhancing the specific surface area of the composite material. This increase provides more attachment sites for CdS and enhances the reactivity in photocatalytic hydrogen production. The specific surface area and pore structure data for CdS and the CdS-xC materials are provided in the Supporting Information (Table S1), with CdS-60C exhibiting the largest specific surface area of $6.96 \text{ m}^2/\text{g}$. The pore size distribution of CdS-60C is illustrated in Supplementary Figure S1. The reason may be that alkaline etching treatment increased the pores of the orange peel biochar itself, increased the specific surface area of the material, provided more attachment points for CdS, and improved the reactivity of photocatalytic hydrogen production. The specific surface area of CdS and CdS-xC and the pore structure data of the materials are shown in Supplementary Table S1. The CdS-60C material had the relatively largest specific surface area of $6.96 \text{ m}^2/\text{g}$. The pore size distribution map of CdS-60C is shown in Supplementary Figure S1.

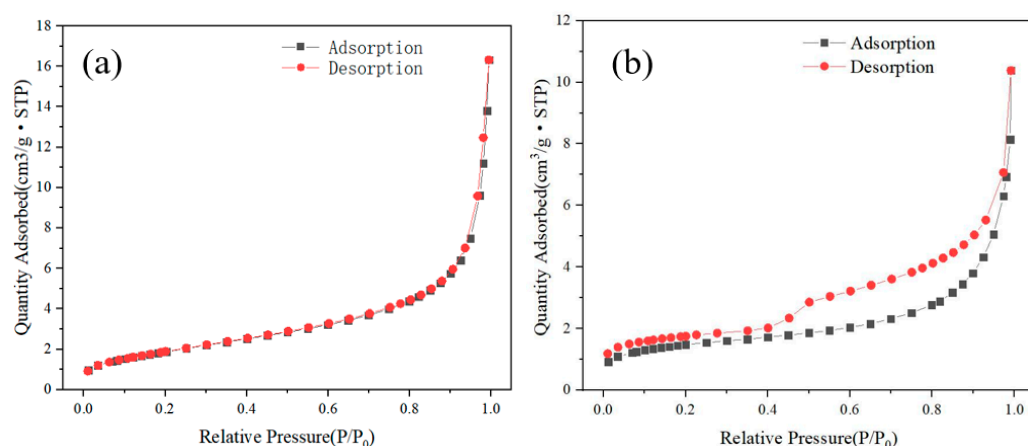


Figure 2. N_2 adsorption–desorption isotherms of CdS (a) and N_2 adsorption–desorption isotherms of CdS-60C (b).

The UV–visible diffuse reflectance spectral images of CdS and 20%, 40%, 60%, and 80% orange peel biomass char-loaded CdS materials are shown in Figure 3a. The spectra show slight differences in absorption characteristics among the various composites. Pure CdS exhibits a strong absorption band edge at about 550 nm, which is related to the intrinsic band gap absorption. Furthermore, Figure 3b shows the band gaps (E_g) of the CdS-60C composite and pure CdS, which are about 1.95 eV and 2.21 eV, respectively [57]. In the CdS-xC system, increasing the biochar content from orange peel narrowed the composite material's band gap, resulting in stronger visible light absorption compared to pure CdS, with the absorption peak shifting towards the red and becoming more pronounced. This redshift and enhancement in visible light absorption are primarily due to the incorporation of orange peel biochar, which alters the material's appearance by darkening its color, thereby enhancing its visible light absorption efficiency. Generally, as the biochar ratio increases, the material's visible light absorption band widens, and the band edge experiences a redshift. This suggests that biochar is an effective support for CdS, significantly enhancing visible light absorption, reducing the band gap, and markedly improving the photocatalytic hydrogen production performance. Orange peel biochar shows a broader visible light absorption band, as shown in Figure S2 in the Supporting Information.

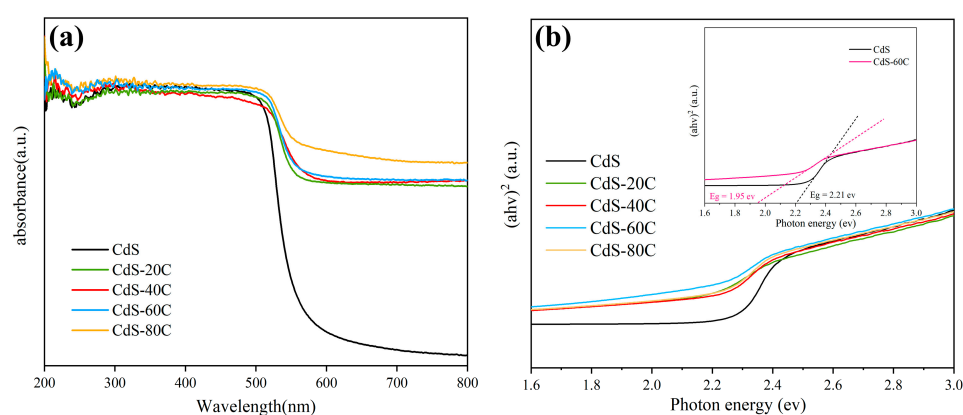


Figure 3. UV–Vis DRS spectra (a) and K-M plots (b) of CdS and CdS-xC composite materials.

To further analyze the materials, the CdS-60C composite was observed by transmission electron microscopy (TEM). Figure 4 presents TEM images of CdS-60C. It is obvious that the orange peel biochar exhibits a multi-layered sheet structure with many small pores on its surface, which provides a very good site for the growth of CdS (Figure 4a,b). The CdS is distributed on the orange peel biochar, and they show very good binding properties (Figure 4c,d). The crystal structure characteristics of the CdS-60C sample were further

examined using high-resolution TEM (HRTEM) (Figure 4f–h). The lattice spacings of the CdS-60C material are 0.335 nm and 0.356 nm, corresponding to the (002) and (100) crystal planes of cubic phase CdS, respectively. Moreover, the uniform distribution of CdS nanoparticles on the orange peel biochar can reduce the aggregation of nanoparticles and provide more reactive sites, which can enhance the photocatalytic performance.

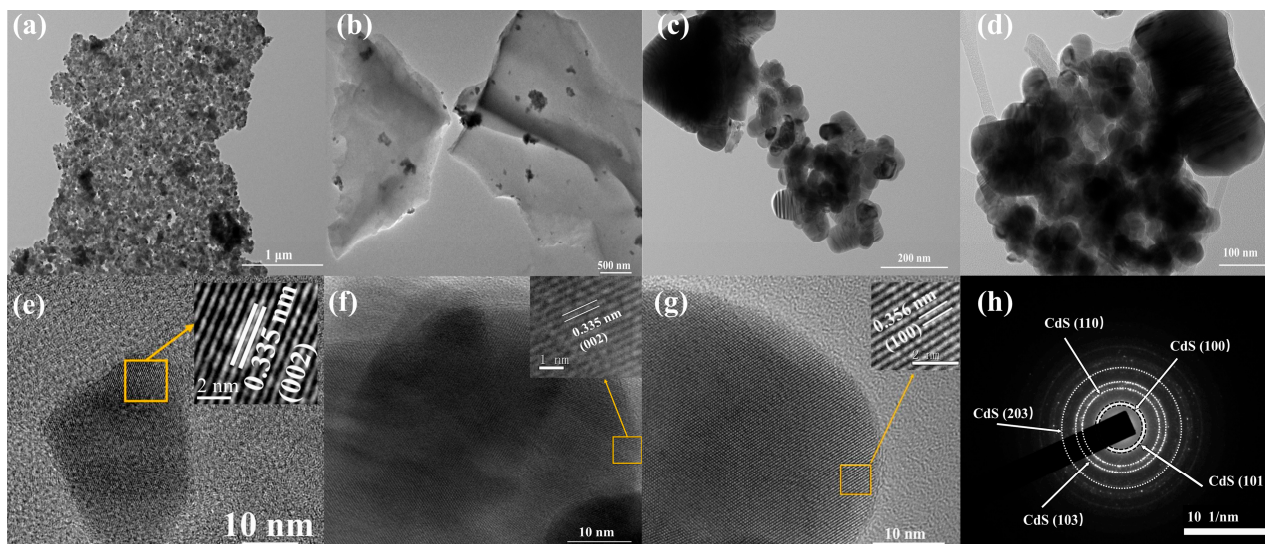


Figure 4. TEM (a–d), HRTEM (e–g), and the corresponding SAED (h) images of CdS-60C.

In order to explore the mechanism of the improved efficiency of CdS-60C's photocatalytic hydrogen production, photoluminescence spectroscopy was used to investigate photogenerated electron–hole generation and transport in the composites. As shown in Figure 5, pure CdS exhibits a broad green emission band and a strong red emission band, with an excitation wavelength of 450 nm. However, the luminescence intensity of CdS-60C decreases sharply compared with pure CdS, which suggests that the successful interfacial contact can effectively transport the photogenerated carriers and hinder the recombination of electron–hole pairs in CdS.

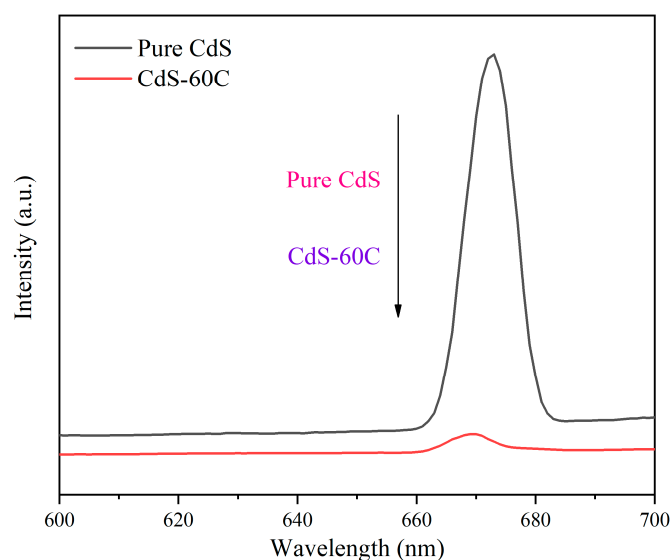


Figure 5. PL spectra of pure CdS and CdS-60C composite.

The ability to achieve efficient photogenerated electron–hole separation and transfer is a very critical factor in improving the photocatalytic hydrogen production activity of a

material. The speed of separation and transfer of photoelectron–hole pairs of a material can be obtained from the side by measuring the transient photocurrent of the material. The transient photocurrent response curves of CdS and CdS-60C are shown in Figure 6. It can be seen from the image that the photocurrent of the CdS-60C composite material increases significantly compared with pure CdS. Obviously, biochar acts as a temporary receiver of photogenerated electrons and can quickly absorb a large number of photogenerated electrons generated on the CdS surface. At the same time, biochar can also effectively inhibit the rapid recombination of photogenerated electron–hole pairs, so that under the same external conditions, CdS-60C has a stronger photocurrent; thus, the material has better photocatalytic activity.

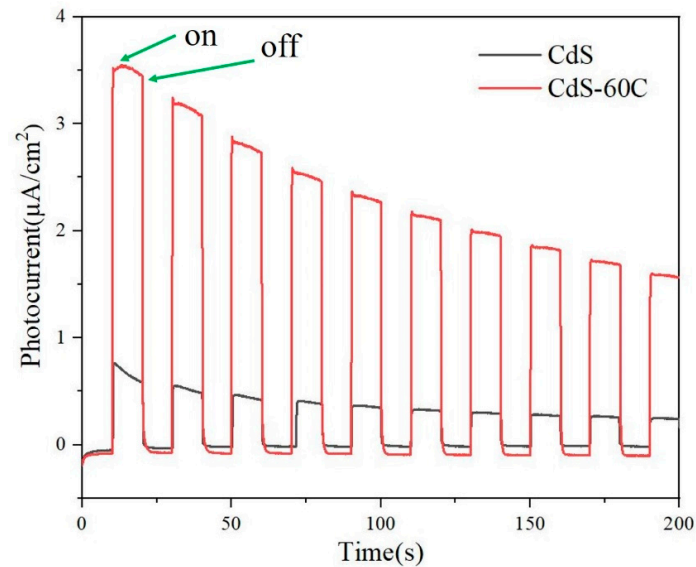


Figure 6. Transient photocurrent response test images for CdS and CdS-60C.

Electrochemical impedance spectroscopy (EIS) was used to further confirm that CdS-60C has a faster electron transfer rate. As shown in Figure 7, from the curve we can see that the curvature radius of the CdS-60C material is lower than that of pure CdS, which indicates that the resistance of the CdS-60C material is lower. These results fully demonstrate the advantages of orange peel biochar in charge loading transfer and recombination delay and explain the improved photocatalytic activity of CdS-60C.

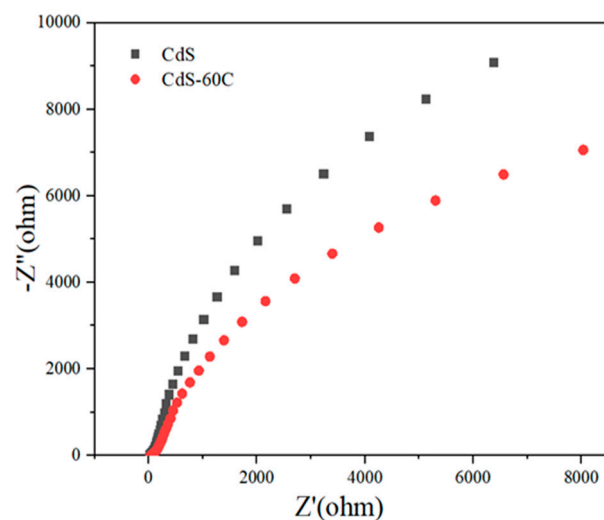


Figure 7. Electrochemical AC impedance of CdS and CdS-60C.

2.2. Hydrogen Production Testing of Materials

Under equivalent sunlight irradiation, the production distribution diagram of photocatalytic hydrogen production by CdS and CdS-xC in each period is illustrated in Figure 8. Each material in the system underwent photocatalysis to produce hydrogen for 4 h under identical lighting conditions. Among them, the hydrogen production rate of pure CdS was $2.11 \text{ mmol}\cdot\text{g}^{-1}\cdot\text{h}^{-1}$. Notably, the material with the highest hydrogen rate in this system was CdS-60C, achieving $7.8 \text{ mmol}\cdot\text{g}^{-1}\cdot\text{h}^{-1}$ under visible light conditions, which is 3.69 times higher than the pure CdS hydrogen production rate. Furthermore, compared with pure CdS, the hydrogen production rates of the composite materials with varying proportions of biochar in the system increased to different degrees. Specifically, their hydrogen production rates were $2.8 \text{ mmol}\cdot\text{g}^{-1}\cdot\text{h}^{-1}$, $4.3 \text{ mmol}\cdot\text{g}^{-1}\cdot\text{h}^{-1}$, $7.8 \text{ mmol}\cdot\text{g}^{-1}\cdot\text{h}^{-1}$, and $4.1 \text{ mmol}\cdot\text{g}^{-1}\cdot\text{h}^{-1}$, respectively, representing increases of 1.33, 2.04, 3.69, and 1.94 times compared with the blank control group. Besides, the comparison of the photocatalytic H₂ production performance of other heterojunction and CdS reported previously in the literature is shown in Table S3 [58–67], demonstrating that CdS-60C has the advantage in pure water systems.

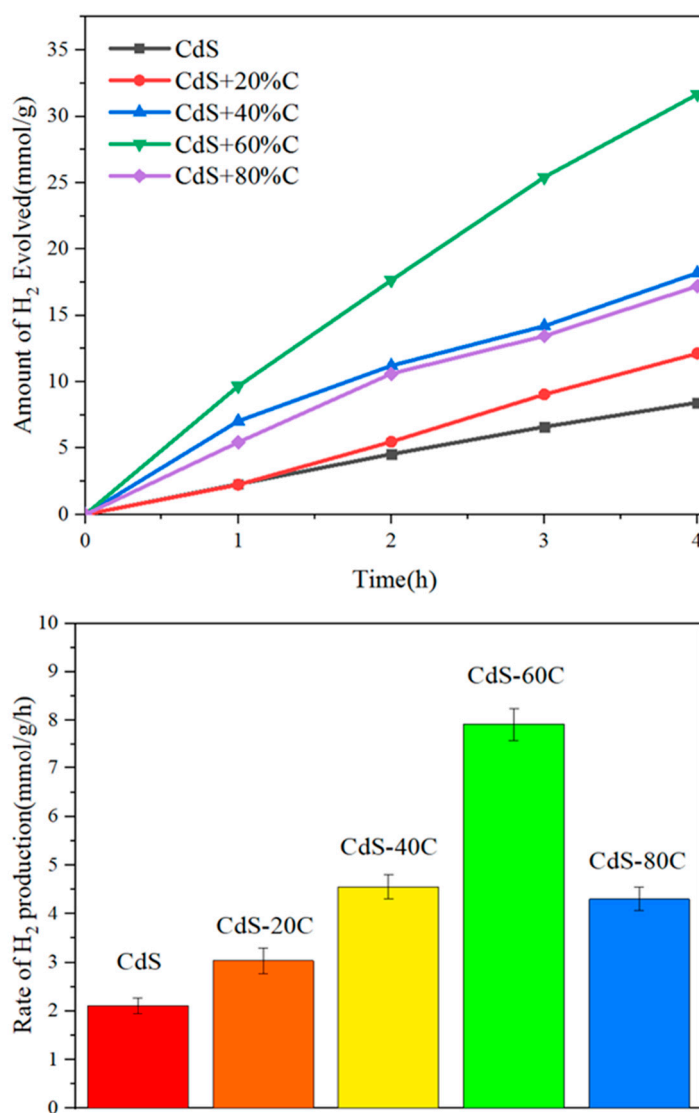


Figure 8. Visible light catalytic hydrogen production efficiency diagram of CdS and CdS-xC (x = 20, 40, 60, 80).

2.3. Cyclic Stability Testing of Materials for Photocatalytic Hydrogen Production

To assess the stability of the photocatalyst, a photocatalytic hydrogen production cycle test was conducted on CdS-60C. As depicted in Figure 9a, after three consecutive cycles of photocatalytic hydrogen production over 12 h, the hydrogen production rate of CdS-60C remained at $25.2 \text{ mmol} \cdot \text{g}^{-1} \cdot \text{h}^{-1}$, representing 83% of the initial hydrogen production rate. It is worth noting that due to the consumption of sacrificial agents in each cycle, the rate of H_2 release tended to decrease. However, upon replacing the sacrificial agent, the photocatalytic hydrogen evolution activity of the CdS-60C composite was restored, indicating its good photostability. After the cycling experiments, the XRD patterns of the regenerated samples were almost the same as those of the fresh ones. As shown in Figure 9b, after three cycles, the crystal structure of CdS did not change, but the intensity of some characteristic peaks weakened, which indicated that the prepared photocatalysts had good stability and recyclability. The slight decrease in photocatalytic efficiency may be caused by partial loss of the photocatalyst during washing.

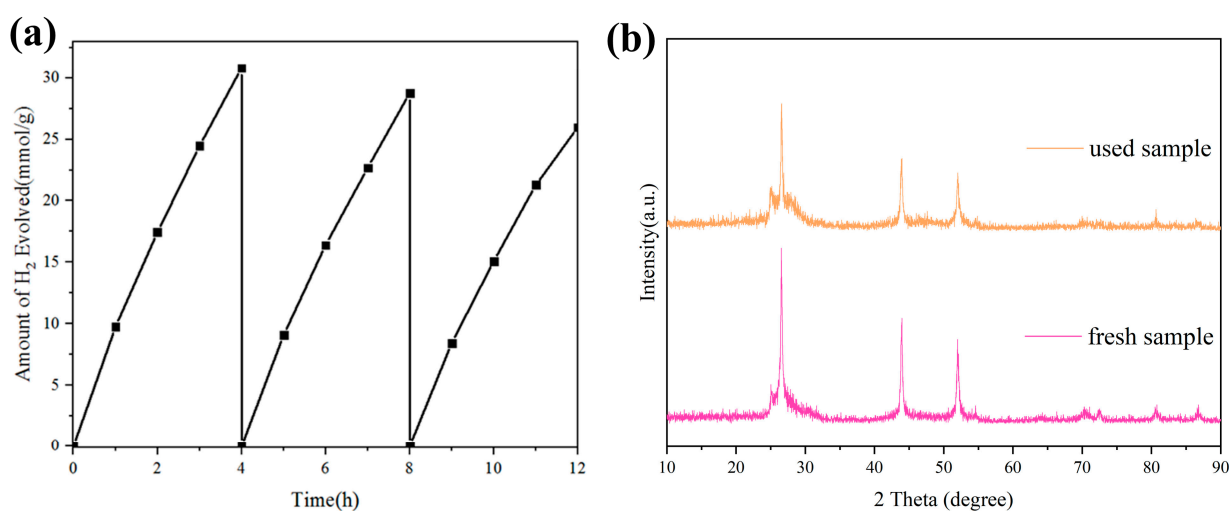
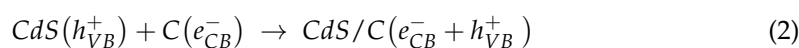
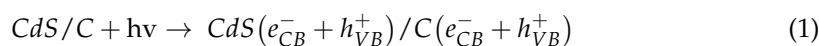


Figure 9. Cycle stability experiment diagram of CdS-60C (a) and XRD pattern of CdS-60C composite after three cyclic tests (b).

2.4. Reaction Mechanism of Photocatalytic Decomposition of Water for Hydrogen Production

Through the summary of the above experiments and characterizations, it becomes evident that the addition of orange peel biochar not only altered the color appearance of CdS but also influenced its photocatalytic hydrogen production rate and cycle stability. The potential mechanism of the photocatalytic hydrogen evolution reaction of the CdS-60C composite is depicted in Figure 10. Upon exposure to light, CdS is excited by visible light, generating electrons and holes. These electrons can transfer from CdS to biochar, where hydrogen ions in the water can accept the electrons and undergo reduction to release hydrogen, thus enhancing the photocatalytic hydrogen evolution performance. The results of the transient photocurrent response, PL spectra, and EIS experiments further support these findings. Additionally, biochar exhibits a strong photothermal effect due to its efficient absorption of near-infrared light, thereby kinetically promoting the photocatalytic hydrogen production reaction by increasing the local temperature. Moreover, under simulated sunlight irradiation, the principal reactions of CdS-60C heterojunction photocatalytic decomposition of aqueous hydrogen in solution are as follows:



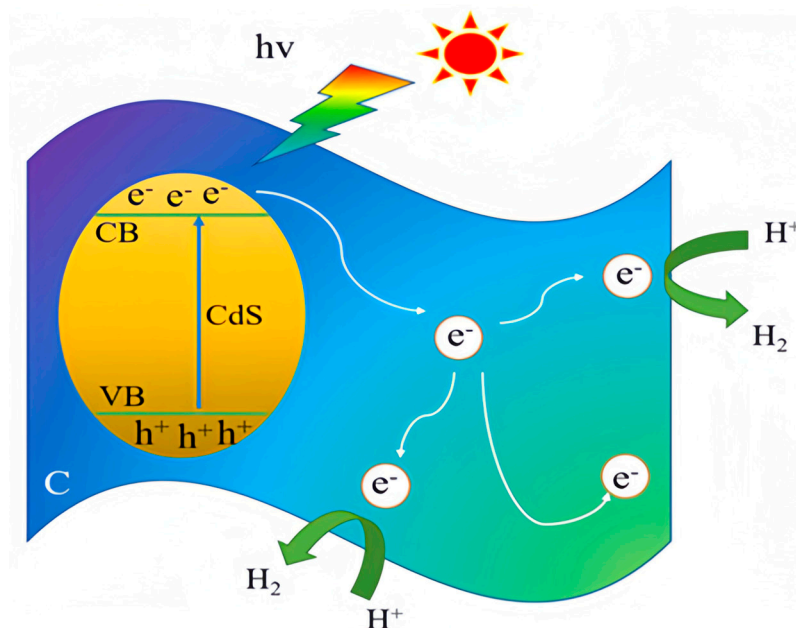


Figure 10. Photocatalytic hydrogen production mechanism of CdS-60C.

3. Experimental

3.1. Preparation of Biochar Material from Orange Peels

The schematic diagram of the preparation of the orange peel biocarbon material is shown in Figure 11. Firstly, citrus peels were collected and dried thoroughly in the sunlight on a sunny day. The dried orange peels were thoroughly crushed with a grinder to produce an orange-colored fine powder after processing. Secondly, the powder made from the obtained batch of orange peels was evenly spread into a quartz boat. The quartz boat containing the orange peel powder was placed in a programmable heating tube furnace, with the temperature set at 500 °C, a heating rate of 5 °C/min, and a constant temperature time of two hours at 500 °C. Finally, according to the program, it naturally cooled to room temperature. During the heating period, high-purity nitrogen was continuously passed into the tube furnace as a protective carrier gas, which was used to avoid the occurrence of combustion or even explosion of the orange peel powder when it met with oxygen at high temperatures.



Figure 11. Schematic diagram of the preparation of orange peel biocarbon materials.

The next process was alkaline etching of the orange peel biomass charcoal. The first step was to prepare a potassium hydroxide solution. Here, 11.222 g of potassium hydroxide solid (0.2 mol) was weighed and dissolved in 200 mL of deionized water to obtain a dilute solution of potassium hydroxide (KOH) at a concentration of 1 mol/L. Secondly, the orange peel biochar made in the previous step was sufficiently ground, and 8 g was taken and poured into the solution, while the speed of the magnetometer stirrer was adjusted to 360 r/min for constant stirring of the mixture for 24 h. The purpose of this step was to carry out sufficient alkali etching of the orange peel biomass charcoal, such that a lot of fine pores could be etched on the surface of the orange peel biochar. After the etching was completed, the KOH solution was poured off and the orange peel biomass char was

rinsed with deionized water until the soaking solution was neutral, and then the cleaned orange peel biomass char was freeze-dried. After freeze-drying, the orange peel biomass charcoal was ground again, and the orange peel biochar obtained after sufficient grinding was collected for use in the subsequent steps.

3.2. Preparation of CdS Blank Control Material

First, 70 mL of deionized water, 3 mmol of $\text{Cd}(\text{CH}_3\text{COO})_2 \cdot 2\text{H}_2\text{O}$, and 4 mmol of thiourea were weighed. A stirrer and the weighed deionized water, $\text{Cd}(\text{CH}_3\text{COO})_2 \cdot 2\text{H}_2\text{O}$, and thiourea were added into a 200 mL beaker; the magnetic stirrer was turned on with the rotational speed adjusted to 450 r/min, and the stirring process lasted 6 h. The stirring process was carried out in the same order. After the stirring was completed, the solution was poured into a reactor liner made of polytetrafluoroethylene (PTFE), the reactor liner was covered and put into the steel sleeve of the reactor, and the lid of the steel sleeve was tightened to ensure that it had been fully sealed. The reaction kettle was placed in the oven at a temperature of 170 °C, and the reaction time was set to 20 h. After the reaction was completed, the orange-yellow product obtained in the reaction kettle was transferred to a centrifuge tube and washed at least three times with 99.5% ethanol and ultrapure water; then, the product was placed in an oven, and the drying temperature was set at 60 °C for 10 h. After the materials were thoroughly dried, the materials were fully ground and the powdered samples were collected, sealed, and stored away from light for subsequent photocatalytic hydrogen production performance testing and characterization analysis.

3.3. Preparation of CdS-C Composites

The weighing and operation of the sulfur and cadmium sources were the same as in Section 3.2. In order to obtain the theoretical content of CdS in the composite, i.e., 20%, 40%, 60%, and 80%, calculated based on the theoretical yield, the corresponding amount of biochar used was 57.79 mg, 115.48 mg, 173.37 mg, and 231.16 mg, respectively. The weighed biochar was added to the beaker along with the sulfur source and cadmium source and stirred. After the stirring was completed, the solution was transferred to a reaction kettle, sealed, and placed in an oven with the temperature set at 170 °C and the reaction time at 20 h. The obtained samples based on the theoretical content of CdS in the composite were marked as CdS-20C, CdS-40C, CdS-60C, and CdS-80C, respectively.

3.4. Characterizations

The crystal structure was analyzed using X-ray diffraction (XRD) (Rigaku Co., Tokyo, Japan) with $\text{Cu K}\alpha$ radiation at a running voltage of 36 kV and a 20 mA current. The sample morphology, elemental mapping, and lattice fringes were examined using transmission electron microscopy (TEM) (JEM-2100, Tokyo, Japan). UV-visible diffuse reflectance spectroscopy (UV-2401PC, Shimadzu, Tokyo, Japan) was used to record the light absorption spectra. The Brunauer–Emmett–Teller (BET) (Micromeritics, Norcross, GA, USA) specific surface area of the samples was determined using a Micromeritics ASAP 2460 nitrogen adsorption–desorption machine. The photoelectrochemical measurements, including photocurrent response (i-t) and electrochemical impedance (EIS), were taken using an electrochemical workstation (CHI-760D, Huake Putian Technology, Beijing, China). The photoluminescence (PL) spectra were recorded on an F97 Pro spectrophotometer (Lengguang Tech., Shanghai, China).

3.5. Photocatalytic Hydrogen Evolution

The photocatalytic hydrogen production activity through water splitting was assessed in a professional system (LabSolar-IIAG, Perfectlight, Beijing, China). In the typical progress, 0.1 mol Na_2SO_3 and 0.05 mol $\text{Na}_2\text{S} \cdot 9\text{H}_2\text{O}$ were dissolved in a reactor filled with 100 mL ultrapure water to form a homogeneous solution. Then, 20 mg of photocatalyst was uniformly dispersed in the solution and with stirring maintained. Before the measurement, the reactor needed to be degassed for half an hour to ensure that the pressure was less than

−0.12 MPa. During the photocatalytic hydrogen evolution reaction, the suspension was carried out under a 300 W xenon lamp (CEL-HFX300, Aulight, Beijing, China) with a UV-IR cut-420 filter and cooled to 10 °C with condensed water. Finally, an online GC-9750 gas chromatograph (GC, China Fuli, nitrogen as carrier gas and 5A molecular sieve column) was used to collect and detect the amount of H₂ precipitated at 1-h intervals.

4. Conclusions

In summary, orange peel biochar-supported cadmium sulfide composites (CdS-C) with prominent light absorption performance were prepared using a combined hydrothermal and calcination method. Orange peel biochar incorporation not only increased the photocatalytic H₂ production rates but also greatly reduced the agglomeration of the material itself and improved the cycling stability. The large surface area of the biochar also provided ample space for reactions to occur. It was found that the hydrogen production efficiency of the CdS-C series materials was significantly improved compared to that of CdS without biochar. In particular, CdS-C with 60% CdS in the composite exhibited the highest photocatalytic activity at 7.8 mmol·g^{−1}·h^{−1}, which is about 3.69 times that of pure CdS. It was still stable after three consecutive cycles, indicating that the biochar improved the photostability of the CdS. Semiconductor-loaded biocarbon-based structures have excellent photocatalytic hydrogen production efficiency, paving the way for important potential applications in visible light hydrogen evolution.

Supplementary Materials: The following supporting information can be downloaded at: <https://www.mdpi.com/article/10.3390/inorganics12060156/s1>, Figure S1. Aperture distribution of CdS-60C; Figure S2. UV-vis DRS spectra of the orange peels biochar. Table S1. Specific surface area and pore structure data of CdS and CdS-xC (x = 20, 40, 60, 80). Table S2. Hydrogen production rates of CdS and CdS(x = 20,40,60,80) normalized by BET surface. Table S3. Comparison of photocatalytic H₂ production with other photocatalysts.

Author Contributions: Conceptualization, X.L. and J.W.; methodology, X.L. and M.H.; experimental, Y.Z.; validation, M.H.; investigation, J.Z. (Jindi Zhang); resources, L.Z. and J.W.; data curation, Y.Z.; writing—original draft preparation, X.L.; writing—review and editing, J.W.; visualization, J.Z. (Jing Zhang); supervision, L.Z. and J.W.; funding acquisition, J.W. All authors have read and agreed to the published version of the manuscript.

Funding: This research received no external funding.

Data Availability Statement: The original contributions presented in the study are included in the article, further inquiries can be directed to the corresponding author.

Acknowledgments: This work was supported by a project from the Department of Ecology and Environment of Yunnan Province (202305AM340008), an R&D Project (2022 No. 4) from the Water Resources Department of Yunnan Province, the Key Laboratory of Advanced Materials for Wastewater Treatment of Kunming (2110304), and the Institute of Frontier Technologies in Water Treatment Co., Ltd., Kunming, 650503, China.

Conflicts of Interest: Authors Jiaqiang Wang and Xiang Li are employed by the company, Institute of Frontier Technologies in Water Treatment Co., Ltd. The remaining authors declare that the research was conducted in the absence of any commercial or financial relationships that could be construed as a potential conflict of interest. The Institute of Frontier Technologies in Water Treatment Co., Ltd. was not involved in the study design, collection, analysis, interpretation of data, the writing of this article or the decision to submit it for publication.

References

1. Yamauchi, M.; Saito, H.; Sugimoto, T.; Mori, S.; Saito, S. Sustainable organic synthesis promoted on titanium dioxide using coordinated water and renewable energies/resources. *Coord. Chem. Rev.* **2022**, *472*, 214773–214802. [[CrossRef](#)]
2. Liao, G.; Gong, Y.; Zhang, L.; Gao, H.; Yang, G.; Fang, B. Semiconductor polymeric graphitic carbon nitride photocatalysts: The “holy grail” for the photocatalytic hydrogen evolution reaction under visible light. *Energy Environ. Sci.* **2019**, *12*, 2080–2147. [[CrossRef](#)]

3. Zhao, Z.; Ge, G.; Zhang, D.; Cheng, B.; Yu, J. Heteroatom-Doped Carbonaceous Photocatalysts for Solar Fuel Production and Environmental Remediation. *ChemCatChem* **2018**, *10*, 62–123. [[CrossRef](#)]
4. Kuang, P.; Sayed, M.; Fan, J.; Cheng, B.; Yu, J. 3D Graphene-Based H₂-Production Photocatalyst and Electrocatalyst. *Adv. Energy Mater.* **2020**, *10*, 1–53. [[CrossRef](#)]
5. Tang, S.; Xia, Y.; Fan, J.; Cheng, B.; Yu, J.; Ho, W. Enhanced photocatalytic H₂ production performance of CdS hollow spheres using C and Pt as bi-cocatalysts. *J. Catal.* **2021**, *42*, 743–752. [[CrossRef](#)]
6. Zhang, Y.; Su, C.; Chen, J.; Huang, W.; Lou, R. Recent progress of transition metal-based biomass-derived carbon composites for supercapacitor. *J. Rare Met.* **2023**, *42*, 769–796. [[CrossRef](#)]
7. Jiang, J.; Zhang, Q.; Zhan, X.; Chen, F. Renewable, Biomass-Derived, Honeycomblike Aerogel as a Robust Oil Absorbent with Two-Way Reusability. *ACS Sustain. Chem. Eng.* **2017**, *5*, 10307–10316. [[CrossRef](#)]
8. Fang, X.; Li, W.; Chen, X.; Wu, Z.; Zhang, Z.; Zou, Y. Controlling the microstructure of biomass-derived porous carbon to assemble structural absorber for broadening bandwidth. *Carbon* **2022**, *198*, 70–79. [[CrossRef](#)]
9. Yao, P.; Zhong, W.; Zhang, Z.; Yang, S.; Gong, Z.; Jia, C.; Chen, P.; Cheng, J.; Chen, Y. Surface engineering of biomass-derived carbon material for efficient water softening. *Chem. Eng. Sci.* **2023**, *282*, 119312–119319. [[CrossRef](#)]
10. Chen, G.; Wang, H.; Han, L.; Yang, N.; Hu, B.; Qiu, M.; Zhong, X. Highly efficient removal of U(VI) by a novel biochar supported with FeS nanoparticles and chitosan composites. *J. Mol. Liq.* **2020**, *15*, 45–53. [[CrossRef](#)]
11. Jin, C.; Sun, J.; Chen, Y.; Guo, Y.; Han, D.; Wang, R.; Zhao, C. Sawdust wastes-derived porous carbons for CO₂ adsorption. Part 1. Optimization preparation via orthogonal experiment. *Sep. Purif. Technol.* **2021**, *276*, 119270–119281. [[CrossRef](#)]
12. Wang, Z.; Shen, D.; Wu, C.; Gu, S. State-of-the-art on the production and application of carbon nanomaterials from biomass. *Green Chem.* **2018**, *20*, 5031–5057. [[CrossRef](#)]
13. Jin, C.; Sun, J.; Bai, S.; Zhou, Z.; Sun, Y.; Guo, Y.; Wang, R.; Zhao, C. Sawdust wastes-derived porous carbons for CO₂ adsorption. Part 2. Insight into the CO₂ adsorption enhancement mechanism of low-doping of microalgae. *J. Environ. Chem. Eng.* **2022**, *10*, 108265–108276. [[CrossRef](#)]
14. Wang, L.; Zhang, H.; Wang, Y.; Qian, C.; Dong, Q.; Deng, C.; Jiang, D.; Shu, M.; Pan, S.; Zhang, S. Unleashing ultra-fast sodium ion storage mechanisms in interface-engineered monolayer MoS₂/C interoverlapped superstructure with robust charge transfer networks. *J. Mater. Chem. A* **2020**, *8*, 15002–15011. [[CrossRef](#)]
15. Lu, Y.; Cai, Y.; Zhang, S.; Zhuang, L.; Hu, B.; Wang, S.; Chen, J.; Wang, X. Application of biochar-based photocatalysts for adsorption-(photo)degradation/reduction of environmental contaminants: Mechanism, challenges and perspective. *Biochar* **2022**, *4*, 45–69. [[CrossRef](#)]
16. Tan, X.; Liu, Y.; Gu, Y.; Xu, Y.; Zeng, G.; Hu, X.; Liu, S.; Wang, X.; Liu, S.; Li, J. Biochar-based nano-composites for the decontamination of wastewater: A review. *Bioresour. Technol.* **2016**, *212*, 318–333. [[CrossRef](#)] [[PubMed](#)]
17. Lee, J.; Park, Y.-K. Applications of modified biochar-based materials for the removal of environment pollutants: A mini review. *Sustainability* **2020**, *12*, 6112–6127. [[CrossRef](#)]
18. Abhijeet, P.; Prem, P.; Chen, X.; Balasubramanian, P.; Chang, S. Activation methods increase biochar's potential for heavy-metal adsorption and environmental remediation: A global meta-analysis. *Sci. Total Environ.* **2023**, *865*, 161252–161262.
19. Talukdar, K.; Jun, B.; Yoon, Y.; Kim, Y.; Fayyaz, A.; Park, C. Novel Z-scheme Ag₃PO₄/Fe₃O₄-activated biochar photocatalyst with enhanced visible-light catalytic performance toward degradation of bisphenol A. *J. Hazard. Mater.* **2020**, *398*, 123025–123034. [[CrossRef](#)]
20. Kumar, A.; Kumar, A.; Sharma, G.; Naushad, M.; Stadler, F.; Ghfar, A.; Dhiman, P.; Saini, R. Sustainable nano-hybrids of magnetic biochar supported g-C₃N₄/FeVO₄ for solar powered degradation of noxious pollutants- Synergism of adsorption, photocatalysis & photo-ozonation. *J. Clean. Prod.* **2017**, *165*, 431–451.
21. He, J.; Chen, L.; Wang, F.; Liu, Y.; Chen, P.; Au, C.; Yin, S. CdS Nanowires Decorated with Ultrathin MoS₂ Nanosheets as an Efficient Photocatalyst for Hydrogen Evolution. *ChemSusChem* **2016**, *9*, 624–630. [[CrossRef](#)] [[PubMed](#)]
22. Hu, Y.; Gao, X.; Yu, L.; Wang, Y.; Ning, J.; Xu, S.; Wen, X.; Lou, D. Carbon-Coated CdS Petaloid Nanostructures with Enhanced Photostability and Photocatalytic Activity. *Angew. Chem.* **2013**, *125*, 5746–5749. [[CrossRef](#)]
23. Kim, M.; Kim, Y.; Lim, S.; Kim, S.; In, S. Efficient visible light-induced H₂ production by Au@CdS/TiO₂ nanofibers: Synergistic effect of core-shell structured Au@CdS and densely packed TiO₂ nanoparticles. *Appl. Catal. B-Environ.* **2015**, *16*, 423–431. [[CrossRef](#)]
24. Li, X.; Dong, H.; Wang, B.; Lv, J.; Xu, G.; Wang, D.; Wu, Y. Controllable Synthesis of MoS₂/h-CdS/c-CdS Nanocomposites with Enhanced Photocatalytic Hydrogen Evolution Under Visible Light Irradiation. *Catal. Lett.* **2018**, *148*, 67–70. [[CrossRef](#)]
25. Wang, X.; Liu, G.; Wang, L.; Chen, Z.; Lu, G.; Cheng, H. ZnO-CdS@Cd Heterostructure for Effective Photocatalytic Hydrogen Generation. *Adv. Energy Mater.* **2012**, *16*, 81–83. [[CrossRef](#)]
26. Yu, X.; Du, R.; Li, B.; Zhang, Y.; Liu, H.; Qu, J.; An, X. Biomolecule-assisted self-assembly of CdS/MoS₂/graphene hollow spheres as high-efficiency photocatalysts for hydrogen evolution without noble metals. *Appl. Catal. B* **2016**, *3*, 51–55.
27. Ye, A.; Fan, W.; Zhang, Q.; Deng, W.; Wang, Y. CdS-graphene and CdS-CNT nanocomposites as visible-light photocatalysts for hydrogen evolution and organic dye degradation. *Catal. Sci. Technol.* **2012**, *2*, 969–978. [[CrossRef](#)]
28. Zhu, C.; Liu, C.; Fu, Y.; Gao, J.; Huang, H.; Liu, Y.; Kang, Z. Construction of CDs/CdS photocatalysts for stable and efficient hydrogen production in water and seawater. *Appl. Catal. B* **2019**, *242*, 78–85. [[CrossRef](#)]

29. Schneider, J.; Bahnemann, D. Undesired Role of Sacrificial Reagents in Photocatalysis. *J. Phys. Chem. Lett.* **2013**, *4*, 3479–3483. [[CrossRef](#)]
30. Kobayashi, Y.; Nishimura, T.; Yamaguchi, H.; Tamai, N. Effect of Surface Defects on Auger Recombination in Colloidal CdS Quantum Dots. *J. Phys. Chem. Lett.* **2011**, *2*, 1051–1055. [[CrossRef](#)]
31. Chakraborty, S.; Mondal, P.; Makkar, M.; Moretti, L.; Cerullo, G.; Viswanatha, R. Transition Metal Doping in CdS Quantum Dots: Diffusion, Magnetism, and Ultrafast Charge Carrier Dynamics. *Chem. Mater.* **2023**, *35*, 2146–2154. [[CrossRef](#)]
32. Wang, P.; Xu, S.; Wang, J.; Liu, X. Photodeposition synthesis of CdS QDs-decorated TiO₂ for efficient photocatalytic degradation of metronidazole under visible light. *J. Mater. Sci. Mater. Electron.* **2020**, *31*, 19797–19808. [[CrossRef](#)]
33. Feng, Y.; Li, J.; Ye, S.; Gao, S.; Cao, R. Growing COFs in situ on CdS nanorods as core–shell heterojunctions to improve the charge separation efficiency. *Sustain. Energy Fuels* **2022**, *6*, 5089–5099. [[CrossRef](#)]
34. Bera, R.; Dutta, A.; Kundu, S.; Polshettiwar, V.; Patra, A. Design of a CdS/CdSe Heterostructure for Efficient H₂ Generation and Photovoltaic Applications. *J. Phys. Chem. C* **2018**, *122*, 12158–12167. [[CrossRef](#)]
35. Korake, P.; Achary, S.; Gupta, N. Role of aliovalent cation doping in the activity of nanocrystalline CdS for visible light driven H₂ production from water. *Int. J. Hydrogen Energy* **2015**, *40*, 8695–8705. [[CrossRef](#)]
36. Huang, S.; Lin, Y.; Yang, J.; Li, X.; Zhang, J.; Yu, J.; Shi, H.; Wang, W.; Yu, Y. Enhanced photocatalytic activity and stability of semiconductor by Ag doping and simultaneous deposition: The case of CdS. *RSC Adv.* **2013**, *3*, 20782–20792. [[CrossRef](#)]
37. Huang, G.; Zhu, Y. Enhanced photocatalytic activity of ZnWO₄ catalyst via fluorine doping. *J. Phys. Chem. C* **2007**, *111*, 11952–11958. [[CrossRef](#)]
38. Reddy, D.; Park, H.; Ma, R.; Kumar, D.; Lim, M.; Kim, T. Heterostructured WS₂-MoS₂ ultrathin nanosheets integrated on CdS nanorods to promote charge separation and migration and improve solar-driven photocatalytic hydrogen evolution. *ChemSusChem* **2017**, *10*, 1563–1570. [[CrossRef](#)] [[PubMed](#)]
39. Reddy, D.; Choi, J.; Lee, S.; Kim, Y.; Hong, S.; Kumar, D.; Kim, T. Hierarchical dandelion-flower-like cobalt-phosphide modified CdS/reduced graphene oxide-MoS₂ nanocomposites as a noble-metal-free catalyst for efficient hydrogen evolution from water. *Catal. Sci. Technol.* **2016**, *6*, 6197–6206. [[CrossRef](#)]
40. Yuan, Y.; Li, Z.; Wu, S.; Chen, D.; Yang, L.; Cao, D.; Tu, W.; Yu, Z.; Zou, Z. Role of two-dimensional nanointerfaces in enhancing the photocatalytic performance of 2D–2D MoS₂/CdS photocatalysts for H₂ production. *Chem. Eng. J.* **2018**, *350*, 335–343.
41. Li, L.; Wu, J.; Liu, B.; Liu, X.; Li, C.; Gong, Y.; Huang, Y.; Pan, L. NiS sheets modified CdS/reduced graphene oxide composite for efficient visible light photocatalytic hydrogen evolution. *Catal. Today* **2018**, *315*, 110–116. [[CrossRef](#)]
42. Zhang, L.; Zhang, C.; Li, J.; Sun, K.; Zhang, J.; Huang, M.; Wang, J. Hydrothermally prepared unactivated bean sprouts biochar supported CdS with significantly enhanced photocatalytic hydrogen evolution activity. *Catal. Commun.* **2024**, *187*, 106861–106869. [[CrossRef](#)]
43. Kang, F.; Shi, C.; Li, W.; Eqi, M.; Liu, Z.; Zheng, X.; Huang, Z. Honeycomb like CdS/sulphur-modified biochar composites with enhanced adsorption-photocatalytic capacity for effective removal of rhodamine B. *J. Environ. Chem. Eng.* **2022**, *10*, 106942–106953. [[CrossRef](#)]
44. Banerjee, R.; Pal, A.; Ghosh, D.; Ghosh, A.; Nandi, M.; Biswas, P. Improved photocurrent response, photostability and photocatalytic hydrogen generation ability of CdS nanoparticles in presence of mesoporous carbon. *Mater. Res. Bull.* **2021**, *134*, 111085–111093. [[CrossRef](#)]
45. Shi, C.; An, Y.; Gao, G.; Xue, J.; Algadi, H.; Huang, Z.; Guo, Z. Insights into Selective Glucose Photoreforming for Coproduction of Hydrogen and Organic Acid over Biochar-Based Heterojunction Photocatalyst Cadmium Sulfide/Titania/Biochar. *ACS Sustain. Chem. Eng.* **2024**, *12*, 2538–2549. [[CrossRef](#)]
46. Huang, H.; Wang, Y.; Jiao, W.; Cai, F.; Shen, M.; Zhou, S.; Cao, H.; Lü, J.; Cao, R. Lotus-Leaf-Derived Activated-Carbon-Supported Nano-CdS as Energy-Efficient Photocatalysts under Visible Irradiation. *ACS Sustain. Chem. Eng.* **2018**, *6*, 7871–7879. [[CrossRef](#)]
47. Norouzi, O.; Kheradmand, A.; Jiang, Y.; Maria, F.; Masek, O. Superior activity of metal oxide biochar composite in hydrogen evolution under artificial solar irradiation: A promising alternative to conventional metal-based photocatalysts. *Int. J. Hydrogen Energy* **2019**, *44*, 28698–29708. [[CrossRef](#)]
48. Chen, D.; Wang, X.; Zhang, X.; Yang, Y.; Xu, Y.; Qian, G. Facile fabrication of mesoporous biochar/ZnFe₂O₄ composite with enhanced visible-light photocatalytic hydrogen evolution. *Int. J. Hydrogen Energy* **2019**, *44*, 19967–19977. [[CrossRef](#)]
49. Qian, J.; Chen, Z.; Sun, H.; Chen, F.; Xu, X.; Wu, P.; Li, P.; Ge, W. Enhanced photocatalytic H₂ production on three-dimensional porous CeO₂/Carbon nanostructure. *ACS Sustain. Chem. Eng.* **2018**, *8*, 9691–9698. [[CrossRef](#)]
50. Zhou, M.; Zhang, K.; Chen, F.; Chen, Z. Synthesis of biomimetic cerium oxide by bean sprouts bio-template and its photocatalytic performance. *J. Rare Earths* **2016**, *34*, 683–688. [[CrossRef](#)]
51. Wei, X.; Ou, C.; Fang, S.; Zheng, X.; Zheng, G.; Guan, X. One-pot self-assembly of 3D CdS-graphene aerogels with superior adsorption capacity and photocatalytic activity for water purification. *Powder Technol.* **2019**, *345*, 213–222. [[CrossRef](#)]
52. Huang, H.; Wang, Y.; Cai, F.; Jiao, W.; Zhang, N.; Liu, C.; Cao, H.; Lü, J. Photodegradation of Rhodamine B over biomass-derived activated carbon supported CdS nanomaterials under visible irradiation. *Front. Chem.* **2017**, *5*, 123–133. [[CrossRef](#)] [[PubMed](#)]
53. Lei, Y.; Yang, C.; Hou, J.; Wang, F.; Min, S.; Ma, X.; Jin, Z.; Xu, J.; Lu, G.; Huang, K. Strongly coupled CdS/graphene quantum dots nanohybrids for highly efficient photocatalytic hydrogen evolution: Unraveling the essential roles of graphene quantum dots. *Appl. Catal. B-Environ.* **2017**, *126*, 59–69. [[CrossRef](#)]

54. Zou, L.; Wang, H.; Wang, X. High Efficient Photodegradation and Photocatalytic Hydrogen Production of CdS/BiVO₄ Heterostructure through Z-Scheme Process. *ACS Sustain. Chem. Eng.* **2016**, *6*, 6–10. [[CrossRef](#)]
55. Liu, S.; Ma, Y.; Chi, D.; Sun, Q.; Chen, Q.; Zhang, J.; He, Z.; He, L.; Zhang, K.; Liu, B. Hollow heterostructure CoS/CdS photocatalysts with enhanced charge transfer for photocatalytic hydrogen production from seawater. *Int. J. Hydrogen Energy* **2022**, *47*, 9220–9229. [[CrossRef](#)]
56. Bai, J.; Chen, W.; Shen, R.; Jiang, Z.; Zhang, P.; Liu, W.; Li, X. Regulating interfacial morphology and charge-carrier utilization of Ti₃C₂ modified all-sulfide CdS/ZnIn₂S₄ S-scheme heterojunctions for effective photocatalytic H₂ evolution. *J. Mater. Sci. Technol.* **2022**, *112*, 85–95. [[CrossRef](#)]
57. Bai, J.; Shen, R.; Jiang, Z.; Zhang, P.; Li, Y.; Li, X. Integration of 2D layered CdS/WO₃ S-scheme heterojunctions and metallic Ti₃C₂ MXene-based Ohmic junctions for effective photocatalytic H₂ generation. *Chin. J. Catal.* **2022**, *43*, 359–369. [[CrossRef](#)]
58. Long, H.; Wang, P.; Wang, X.; Chen, F.; Yu, H. Optimizing hydrogen adsorption of NixB cocatalyst by integrating P atom for enhanced photocatalytic H₂-production activity of CdS. *Appl. Surf. Sci.* **2022**, *604*, 154457. [[CrossRef](#)]
59. Lu, H.; Liu, Y.; Zhang, S.; Wan, J.; Wang, X.; Deng, L.; Kan, J.; Wu, G. Clustered tubular S-scheme ZnO/CdS heterojunctions for enhanced photocatalytic hydrogen production. *Mater. Sci. Eng. B* **2023**, *289*, 116282. [[CrossRef](#)]
60. He, K. ZnO/ZnS/CdS three-phase composite photocatalyst with a flower cluster structure: Research on its preparation and photocatalytic activity hydrogen production. *Int. J. Hydrogen Energy* **2024**, *51*, 30–40. [[CrossRef](#)]
61. Liu, Y.; Dai, F.; Zhao, R.; Huai, X.; Han, J.; Wang, L. Aqueous synthesis of core/shell/shell CdSe/CdS/ZnS quantum dots for photocatalytic hydrogen generation. *J. Mater. Sci.* **2019**, *54*, 8571–8580. [[CrossRef](#)]
62. Liu, Z.; Zhuang, Y.; Dong, L.; Mu, H.; Li, D.; Zhang, F.; Xu, H.; Xie, H. Enhancement Mechanism of Photocatalytic Hydrogen Production Activity of CeO₂/CdS by Morphology Regulation. *ACS Appl. Energy Mater.* **2023**, *6*, 7722–7736. [[CrossRef](#)]
63. Qi, Z.; Chen, J.; Li, Q.; Wang, N.; Carabineiro, S.; Lv, K. Increasing the Photocatalytic Hydrogen Generation Activity of CdS Nanorods by Introducing Interfacial and Polarization Electric Fields. *Small* **2023**, *19*, 2303318. [[CrossRef](#)]
64. Liu, J.; Qiu, L.; Liu, Z.; Tang, Y.; Cheng, L.; Chen, Z.; Li, P.; Cao, B.; Chen, X.; Kita, H.; et al. Boosting the photocatalytic activity for H₂ production of Bi₂O₂Se/CdS heterojunction. *Mater. Lett.* **2023**, *345*, 134498. [[CrossRef](#)]
65. Meng, A.; Zhu, B.; Zhong, B.; Zhang, L.; Cheng, B. Direct Z-scheme TiO₂/CdS hierarchical photocatalyst for enhanced photocatalytic H₂ production activity. *Appl. Surf. Sci.* **2017**, *422*, 518–527. [[CrossRef](#)]
66. Kalia, R.; Pirzada, B.; Kunchala, R.; Naidu, B. Noble metal free efficient photocatalytic hydrogen generation by TaON/CdS semiconductor nanocomposites under natural sunlight. *Int. J. Hydrogen Energy* **2023**, *48*, 16246–16258. [[CrossRef](#)]
67. Zhang, L.; Zhu, X.; Zhao, Y.; Zhang, P.; Chen, J.; Jiang, J.; Xie, T. The photogenerated charge characteristics in Ni@NiO/CdS hybrids for increased photocatalytic H₂ generation. *RSC Adv.* **2019**, *9*, 39604–39610. [[CrossRef](#)]

Disclaimer/Publisher's Note: The statements, opinions and data contained in all publications are solely those of the individual author(s) and contributor(s) and not of MDPI and/or the editor(s). MDPI and/or the editor(s) disclaim responsibility for any injury to people or property resulting from any ideas, methods, instructions or products referred to in the content.